

Sedimentation event sensor: New ocean instrument for in situ imaging and fluorometry of sinking particulate matter

Paul R. McGill,* Richard G. Henthorn, Larry E. Bird, Christine L. Huffard, Dennis V. Klimov, Kenneth L. Smith Jr.

Monterey Bay Aquarium Research Institute, Moss Landing, CA USA

Abstract

Measuring the quantity and composition of sinking particulate matter is key to understanding biogeochemical processes in the ocean. This has been done in the past with sequencing sediment traps, which collect and store particulate matter in sample bottles for subsequent laboratory analysis. Having a limited number of bottles, these traditional traps force the user to choose between finer time resolution and longer deployment duration. We have built a new sediment trap that analyzes the collected material in situ, eliminating the need to preserve and store the samples. This new instrument, the Sedimentation Event Sensor (SES), captures macro images of the sample with front and back lighting, and takes fluorometric measurements in two bands as proxies for the presence of chlorophyll *a* and accessory pigments. The SES can process 6200 samples during a single deployment, which is the equivalent of 15 samples per day for more than a year. Here, we describe the design of the SES and present the results of its first three deployments at 3910 m depth. Images and fluorometry data revealed high variability of sinking particulate matter composition on the order of hours. Sedimentation patterns detected by the SES largely agreed with mass flux patterns measured from traditional traps deployed concurrently nearby. Given the functional differences, the SES is best used to complement rather than replace traditional sediment traps.

Resolving biogeochemical cycling in the ocean is heavily dependent on measuring particulate matter fluxes. Funnels and cylinders have been used over the past four decades to collect particulate matter sinking through the water column and to estimate fluxes of biogenic and mineral material in all major regions of the world ocean (Knauer et al. 1979; Honjo 1980). These sediment traps can be either moored at discrete depths through the water column or on autonomous free-drifting devices set to float at predetermined depths or density surfaces (Buesseler et al. 2007). To estimate particle fluxes all of these designs require the retrieval and subsequent laboratory analysis of collected samples, which are typically chemically preserved in situ. Sequencing sediment traps, which open and close a series of collection bottles at preprogrammed times, are typically necessary for producing long time-series collections, but are limited by the

number of sample bottles available (Honjo and Doherty 1988).

Our goal was to develop an instrument, the Sedimentation Event Sensor (SES), that could temporarily capture particulate matter sinking through the water column, make fluorometric measurements to estimate the chlorophyll content of collected particulates, produce high-resolution images of collected particulates, and discard rather than preserve samples for subsequent laboratory analysis. We also required the instrument to be moored at abyssal depths and work at any desired sampling frequency from hours to days for deployment periods of up to a year. The resulting time-series of high-definition images and optical data could then be processed to estimate biological origin, quantity, size distribution, and fluorescent quality of sinking particulate matter without the need to store or preserve samples, or handle toxic preservatives. For biogenic material, the organic carbon and nitrogen content could then be estimated from similar material collected concurrently in conventional sediment traps.

Here, we describe the design of the SES, developed at the Monterey Bay Aquarium Research Institute, and assess mechanical performance and scientific lessons learned from early testing and its first three deployments spanning 21 months.

*Correspondence: mcgill@mbari.org

This is an open access article under the terms of the Creative Commons Attribution-NonCommercial-NoDerivs License, which permits use and distribution in any medium, provided the original work is properly cited, the use is non-commercial and no modifications or adaptations are made.

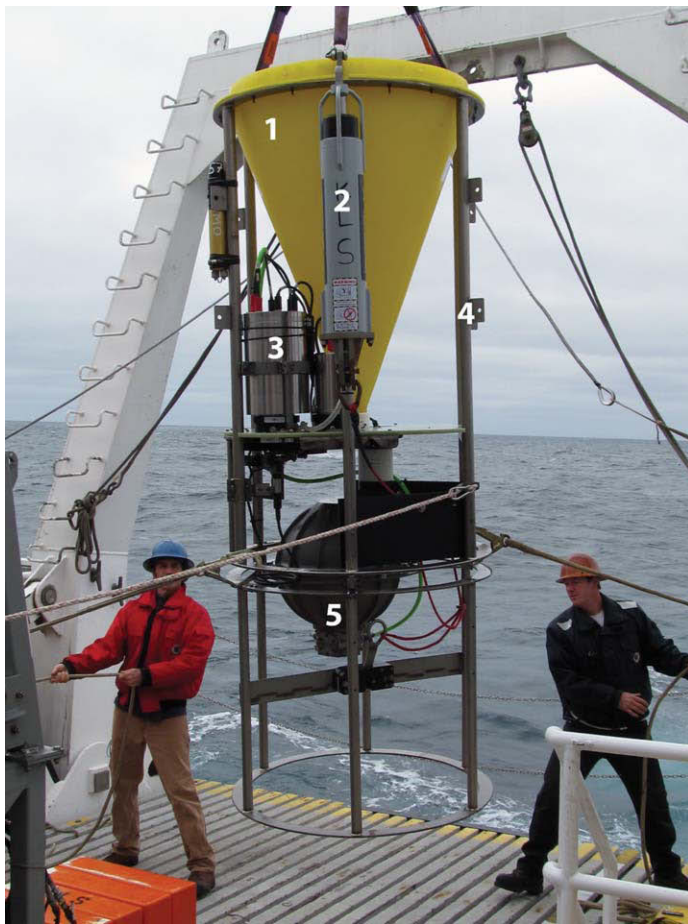


Fig. 1. The SES being prepared for deployment. The instrument is deployed as part of a 140-m-long mooring string. Components shown: (1) funnel, (2) acoustic release, (3) camera and controller housing, (4) titanium frame, (5) battery sphere.

Materials and procedure

Overview

The SES is a stand-alone, self-powered instrument built into an open titanium frame, deployable at depths up to 4000 m. A large plastic funnel collects sinking particulate matter and channels it onto a movable sample plate. After the programmed sample period, the sample plate is positioned under a fluorometer to detect fluorescence consistent with the presence of chlorophyll *a* (Chl *a*) and accessory pigments, and then under a digital camera to record both front- and back-lit images. Finally, the sample is discarded and the sample plate is cleaned by brushes before the empty plate is positioned back under the funnel to collect the next sample.

Mechanical hardware

The core of the SES mechanical design is a commercially available sediment trap (McLane Laboratories model Mark78H-21). The polyethylene sample funnel is 80 cm in diameter with a collection area of 0.5 m². The titanium

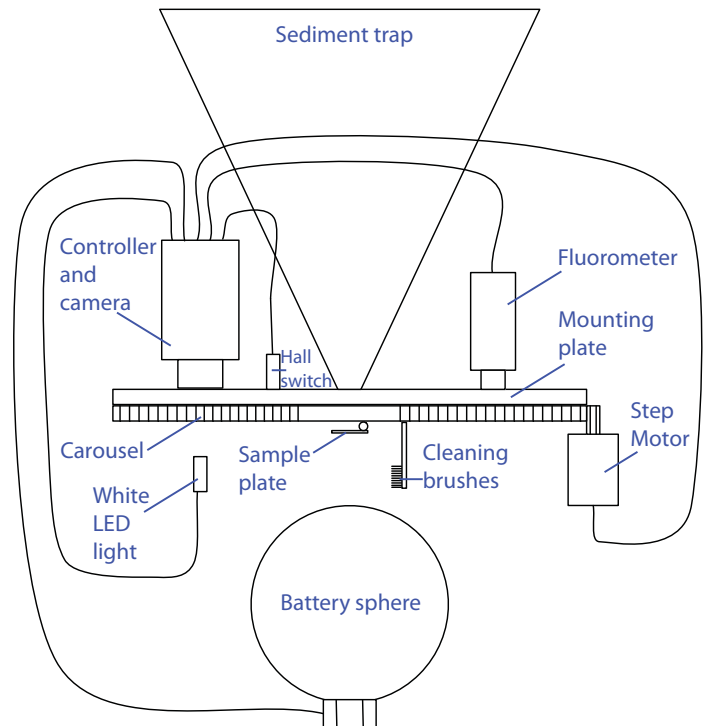


Fig. 2. Placement of major system components. A funnel collects sinking particulate matter, which is then imaged and analyzed by a downward-looking camera and a fluorometer. A large battery, in a titanium sphere, powers the system for more than a year. Components not drawn to scale.

frame (Fig. 1) was modified to function as the bottom-most element in a vertical mooring string, although the instrument can be deployed at any position along a vertical mooring line. A 165 kg steel drop weight on a wire rope holds the SES 50 m above the seafloor, while a series of five 0.11 m³ syntactic foam floats provide buoyancy above the SES. Mounts were added to the frame to accommodate two deep-sea acoustic releases (Teledyne Benthos model 865-A). An auxiliary frame extension, 92 cm in diameter and 78 cm in length, was added to the base of the Parflux frame to accommodate a titanium pressure sphere and drop-weight release mechanism. The titanium pressure sphere contains the necessary electronics and batteries to power the system, and the tandem acoustic release mechanism provides redundancy to drop the ballast weight, allowing the instrument to ascend to the surface for recovery. The instrument weighs 147 kg in water, is 2.61 m in height and 0.92 m in diameter.

Figure 2 shows the relative placement of the SES system components. The existing sample bottle carousel was replaced with a new sample assembly (Fig. 3). This assembly allows the horizontal sample plate, mounted beneath the funnel during the collection period, to rotate into position beneath the fluorometer or camera for analysis or imaging. As the rotation continues, a cam-driven mechanism moves

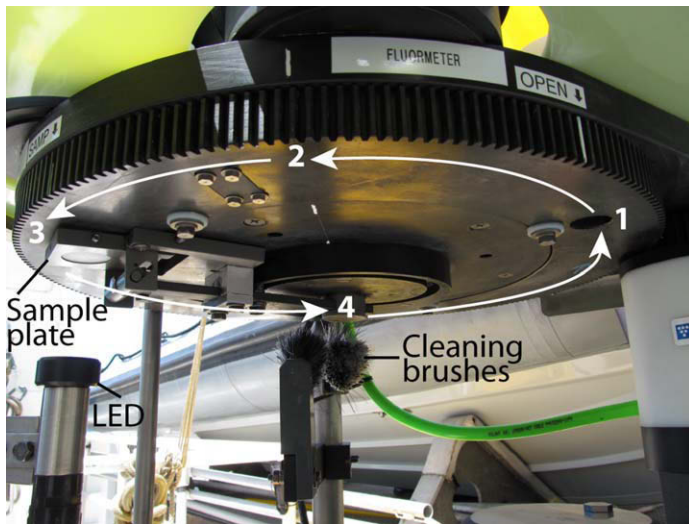


Fig. 3. Carousel assembly viewed from below. Sample bottles have been replaced with a white, translucent sample collection plate, which is rotated through collection (1), fluorometry (2), and imaging (3) stations. A light-emitting diode (LED) light at the lower-left illuminates the sample from below for imaging. After the sample has been analyzed, it is discarded and the sample plate is passed through a set of cleaning brushes (4). The clean sample plate is then rotated back to the base of the funnel to begin collecting the next sample. Alternatively, the carousel can be left in a flow-through position such that the sample plate is not beneath the base of the funnel, and the sinking particulate matter flows through a hole in the carousel plate without being collected. This allows the sample analysis interval to be longer than the collection time to avoid accumulating too much material on the sample plate during long analysis intervals or during times of heavy particulate flux. For example, a sample can be collected for 2 h, followed by a 4-h flow-through mode before collecting another 2-h sample.

the sample plate to a vertical orientation, dumping the sample. The plate then passes between a pair of cleaning brushes to remove any accumulated material before starting the next collection cycle. At the completion of one revolution the sample plate is back in position below the funnel, ready for the next sample collection. The camera and fluorometer housings are mounted near the base of the collection funnel vertically, with their viewports looking down. The battery sphere is centered inside the frame at the bottom of the instrument (Fig. 2). Cleaning brushes have not shown fouling or accumulation of particulates during deployments at Station M. However they are easily replaceable if fouling is an issue at other sites.

Sensors and electronics

Most of the SES sensors and electronics are contained within three titanium pressure housings: two cylindrical housings hold the fluorometer and the camera + system controller, while a spherical case holds the large battery that powers the system (Figs. 2 and 3). The original McLane sediment trap had a simple controller to advance the sample bottle carousel to each position at a programmed interval. A

much more sophisticated controller is required to interface to the SES camera and fluorometer. The new controller uses a PC/104 board stack comprised of an ARM9-based CPU board, a relay board to switch power to the lights and sensors, and an RS-232 serial interface board to connect the sensors to the CPU (Technologic Systems models TS-7250-V2, TS-RELAY8, and TS-SER1). A separate stepper motor controller board (Allmotion model EZ-17) drives the original McLane carousel motor to move the sample plate between the collection, imaging, and fluorometry stations. A Hall-effect switch senses the position of the carousel to index the stations.

A 5-megapixel color digital camera (Allied Vision Technologies model GC2450C) equipped with a 12–36 mm C-mount varifocal video lens (Computar model 11A) captures images of the particulate matter collected on the sample plate. The camera looks down on the sample through a flat-glass viewport. Each pixel in the image represents a distance of 13.9 μm on the 25-mm-diameter sample plate, yielding 72 pixels per mm.

The camera lens is not accessible for adjustment inside the sealed controller housing when the SES is deployed. Therefore the zoom, focus, and aperture of the lens were pre-adjusted on the bench, without the housing, using a test target positioned at the precise distance in air required to simulate the combined optical thickness of the glass viewport and water interface. The measured thickness of the glass and water between the camera lens and sample plate is 113 mm. However, based on the thicknesses and refractive indices of the optical elements, a computer-aided design model of the assembly calculated the in-air optical distance as 82 mm. Once the focus was set to 82 mm, the aperture was adjusted to provide a depth of field that maintains image detail from at least 3.2 mm above the top surface of the sample plate to 1.6 mm below the surface. The camera lens, adjusted using this procedure, required no further readjustments once the SES was submerged.

The sample plate is made of translucent white high-molecular-weight polyethylene to act as a volumetric light diffuser capable of operating underwater and at high ambient pressure. Its thickness is 10 mm, selected as a compromise between light uniformity across the camera field of view and efficiency of light transmission. The 31.5 mm diameter of the plate was selected to be slightly larger than the 25 mm clear viewport aperture to allow for some inaccuracy in the mechanical indexing of the carousel.

Two LED lights illuminate the sample: a ring light surrounds the camera lens inside the housing and illuminates the sample from above, while an external light in its own pressure housing provides illumination through the bottom of the translucent sample plate (Fig. 3). The LEDs in both lights are T-1 $\frac{3}{4}$ Lumex SLX-LX5093UWC/C. The ring light uses eight LEDs positioned at 20 degrees relative to the lens centerline so the light beam of each LED crosses the

centerline and illuminates the opposite side of the plate to eliminate shadows. The external light has a custom titanium pressure housing with an 8-mm-thick flat quartz window. The housing contains three LEDs equally spaced around the centerline with their light beams parallel to the centerline. To achieve a compromise between uniformity of illumination and efficiency of light delivery, the vertical position of the external LED light housing was first adjusted in air to achieve the desired image brightness and uniformity. Then the distance was increased by the ratio of the water-to-air refractive indices to correct for underwater illumination. The final mechanical position of the light source is about 70 mm under the sample plate.

The SES fluorometer was designed to detect the presence of Chl *a* and accessory pigments in the collected samples. This allows the instrument to distinguish phytodetritus from other material. The fluorescence data are acquired by an optical two-band fluorometer that analyzes sediment collected on the sample plate. Built at the Monterey Bay Aquarium Research Institute, the fluorometer is sensitive in the 590×10 nm (590 nm center wavelength with 10 nm bandwidth, full width at half maximum) and 690×10 nm optical bands, which approximate the centers of the Chl *a* and phycoerythrin emission bands respectively (Yentsch and Phinney 1985). The fluorometer is installed in a separate pressure housing connected to the controller housing with underwater cables for power and data signals (Fig. 2). Fluorescence excitation is provided by a blue 470×25 nm LED (Lumileds model LXHL-NB98) followed by a 480×30 nm bandpass filter to minimize crosstalk between optical channels.

The fluorescence detectors are comprised of two photomultiplier tubes (PMTs) each integrated with a high-voltage power supply and interface electronics into a self-contained module (Hamamatsu model H7155 for the 590 nm band, and H7155-01 for the 690 nm band) operating in photon-counting mode. Each PMT has a set of neutral density filters installed in light-tight enclosures along with 590×10 nm and 690×10 nm interference filters immediately in front of each PMT to protect them from possible exposure to bright light. The light paths to the two detectors and the excitation LED are combined by two generic dichroic 25 mm, 45° filters. The first one reflects blue light of wavelengths less than 510 nm from the LED 90° to the sample plate and passes the resulting fluorescence signal to the detectors. The second filter reflects yellow 550–620 nm light to the 590 nm detector, and transmits red light to the 690 nm detector. In addition, a 25 mm aluminum-coated first-surface mirror is used in front of the 590 nm channel PMT to fold the optical path, reducing the size of the fluorometer.

The fluorometer contains a microprocessor to control its functions and to communicate with the computer board stack in the main housing (Fig. 2). The integration time, i.e., the length of time that the excitation LED is on and the PMTs are measuring fluorescence, is programmable from 1 ms to 10 s in 1 ms steps. Measurements can also be made

with the excitation LED off. If the particulate matter sample is not at the fluorometer position, this allows the measurement of the PMTs' dark current, which can be subtracted from the subsequent fluorescence measurement to improve accuracy. If the sample is at the fluorometer position, dark measurements can detect luminescence, or phosphorescence if the sample has just been illuminated by a fluorescence measurement. Raw data from the fluorometer are reported as photomultiplier counts, which we standardized based on excitation duration leading to a sample dataset with the units of photomultiplier counts per second (PMC s^{-1}).

Calibration of the SES fluorometer presents a challenge. Commercially available fluorometers measure chlorophyll in units of $\mu\text{g/L}$, and are presumed to operate in an infinite, homogeneous liquid medium. These fluorometers can be calibrated by placing them in solutions of known chlorophyll concentration. The SES fluorometer, however, measures fluorescence from solid targets of unknown size or distribution at a fixed distance. We could find no solid, calibrated Chl *a* standard target and thus the assignment of metric units to the output cannot be justified. Therefore, the output of the SES fluorometer is presented in photomultiplier counts per second based on measurements with a 1 s integration time. The count rates are interpreted relative to each other and represent the relative presence or absence of fluorescing material in the sample. To test whether an increase in the amount of fluorescent material yielded a linear increase in photomultiplier counts, we fabricated calibration disks containing linearly increasing areas of a dyed acrylic known to provide a stable fluorescence response at both 590 nm and 690 nm. Plexiglas Satinice® plum 4H01 DC (polymethylmethacrylate) was chosen as the reference material because of its photostability and suitable combination of readings by a Chl *a* sensor in another study (Earp et al. 2011). This material is 6 mm thick and was cut to rounds with target areas of 1.0 cm^2 , 2.0 cm^2 , 3.0 cm^2 , and 4.0 cm^2 . Targets were placed in the center of the SES sample plate area. We compared the readings of this reference material to readings of the adaxial surface of a 3.2 cm^2 cutting of a fresh leaf. We did not vary thickness of the reference objects to test for self-shading, which may occur when samples overlap on the sample plate and interfere with the sensor's ability to excite and absorb a signal from underlying particles.

Both the 590 nm and 690 nm fluorescence readings increased with increasing amount of fluorescent reference material on the sample plate (Fig. 4). For the 690 nm band:

$$\text{fluorescent reading}_{\text{ref}690} = 8.0 \text{ PMC s}^{-1} + 25 \times \text{target area}_{\text{ref}} (R^2 = 0.98).$$

Fluorescence readings in the 690 nm band consistently increased with target area for sample plate coverage up to 4 cm. For the 590 nm band, the linear relationship between fluorescence reading and target area was:

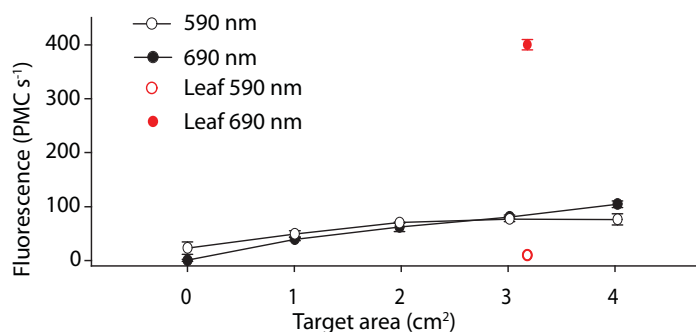


Fig. 4. Fluorescence readings (average ± standard error) for reference targets of varying sizes [black; Plexiglas Satinice® plum 4H01 DC (polymethylmethacrylate)] and a leaf cutting (red) of varying size, based on a 1 s integration time. Open circles show readings at 590 nm, and dots show readings at 690 nm.

$$\text{fluorescence reading}_{\text{ref590}} = 33 \text{ PMC s}^{-1} + 13 \times \text{target area}_{\text{ref}} (R^2 = 0.84).$$

In the 590 nm band, an increase in area beyond 3 cm² did not contribute to additional photomultiplier counts, and background readings were variable when there was no reference material on the sample plate. With no material on the sample plate, readings averaged 0.7 ± 1.8 standard error (SE) PMC s⁻¹ in the 690 nm band and 23 ± 11 SE PMC s⁻¹ in the 590 nm band. We therefore recommend interpreting readings of the 590 nm band with caution when particle coverage is lower than 20% or exceeds 60% of the sample plate. Compared to the reference material, readings of the leaf cutting were higher in the 690 nm band [400 ± 9.6 SE PMC s⁻¹] and lower in the 590 nm band (10 ± 4.3 SE PMC s⁻¹).

Two battery options are available to power the SES. The first option is a 28 V battery comprised of 240 alkaline D cells. The alkaline battery provides about 2500 Wh of energy, which is enough to process more than 1500 sediment samples. The second option is a lithium primary battery which increases the energy capacity to almost 10 kWh to process more than 6200 samples. The SES collects particulate matter for the vast majority of a deployment, so it is critical that all the electronics can be put into a very low-power state while the system is “sleeping” and collections are taking place, or the sample plate is in the pass-through position. This goal is accomplished by a custom power controller board, which has DC-to-DC converters to convert the 28 V battery voltage to the 5 V and 12 V required by the system. The power controller is capable of providing up to 39 W while the system is processing a sample, although the current system uses less than 10 W. Once the sample is processed and the sample plate is back in the collection position, the controller removes power from the rest of the system and enters a sleeping state, consuming less than 1 mW until waking the system for the next

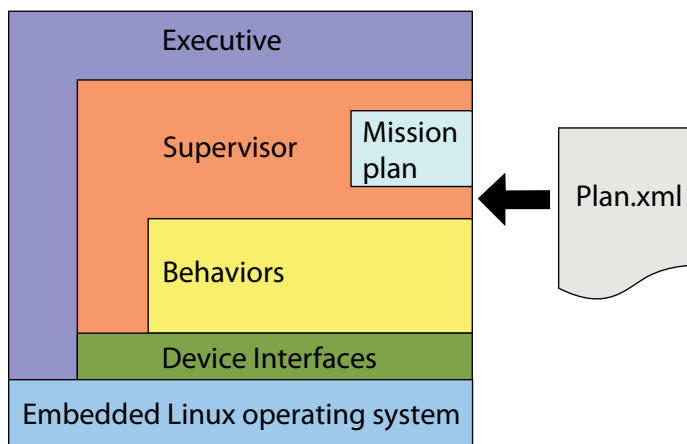


Fig. 5. Diagram of the software architecture, consisting of Ruby and C application code running on a Linux operating system. A mission plan file consisting of a list of Behaviors is read and executed by a Supervisor process.

sample analysis. This approach allows the use of commercial computer boards and sensors that are not optimized for low power consumption, while still keeping the average power consumption of the system low enough for year-long deployments.

Software

The design of the software system used in the SES was driven primarily by the requirement for unattended operations to abyssal depths with long service intervals of up to a year. The system requires reliable operation of the SES components, mission data management, and the capability to resume the mission after scheduled hibernation periods or unscheduled restarts. The resulting system design emphasizes simple, robust functionality over cutting-edge techniques with the objectives of predictable mission programming, minimal energy use, and easy servicing in the field.

Figure 5 is a high-level diagram of the software architecture. Generally, commands flow from the top of the diagram toward the bottom and information is filtered from bottom to the top. Higher-level logic is conducted as you move up in the diagram.

At the base is a stable and reliable Debian-based Linux kernel and operating system tailored for embedded systems. Communication with the sensor and actuator devices is handled using conventional Linux serial and networking protocols, using both C and Ruby programming languages. The SES system design also relies on the simple and proven process management tools available in Linux to both automatically start the control system at boot time, and to restart the system should it fail unexpectedly.

The Behavior layer is where most of the SES control logic resides. Behaviors can be described best as functional units of operation that define what the instrument can be tasked to do. An example of a Behavior is MoveCarousel, which

```

<Plan tarzip="false" name="6-per-day-8-months" sites="1420" >
  <!-- Run through the carousel positions, take images, log fluorometer data -->

  <MoveCarousel name="After Brush" steps="158000" />

  <MoveCarousel name="Before Brush" steps="117000" />

  <MoveCarousel name="Nearly Home" steps="200000" />

  <HomeClean />

  <MoveCarousel name="To Collection" location="collection" />

  <Pause name="2-hr collection" interval="true" hibernate_for="120" />

  <MeasureFluorometry dark_time="1000" ref_time="1000" />

  <MoveCarousel name="To Fluorometry" location="fluoro" />

  <MeasureFluorometry lum_time="1000" flu_time="1000" phos_time="1000" />

  <MoveCarousel name="To Camera" location="camera" />

  <FluorolImage prefix="_pulse61" />

  <!-- Pause here in flow-thru for 2hrs -->
  <Pause name="2-hr collection" interval="true" hibernate_for="120" />

</Plan>

```

Fig. 6. Segment of a mission plan, consisting of a list of behaviors specified sequentially in a text file using a simple markup format. In this case, the markup tags are magenta, tag attribute names are red, attribute values are navy, and comments are green.

moves the carousel to a given position. In the SES control system Behaviors run one at a time, have complete control of the instrument during execution, and leave the instrument in a default state when completed. By leaving the SES in a default state, a user is able to combine behaviors in arbitrary ways to produce unique mission plans.

A Mission Plan is the method by which a user defines the operation of the SES during a deployment. A typical mission consists of the following Behaviors:

1. Rotate the carousel through the cleaning brushes to discard the sample and stop at the sample collection position.
2. Rotate the carousel to the sample-collection position.
3. Sleep for 4 h while the sample is collected.
4. Rotate the carousel to the fluorometer position and make measurements.
5. Rotate the carousel to the camera position and capture images.

These Behaviors are specified sequentially in a text file using a simple markup format. Figure 6 is an example of a mission file. The mission author simply lists the Behaviors to execute in the desired sequence. The names of the different Behavior types (e.g., HomeClean) hint at the function of each Behavior. The Behavior attributes are generally unique to each Behavior type. For example, the location attribute of the MoveCarousel Behavior relates to the position to which the carousel will move.

Mission science data are stored on a 32 GB Compact Flash memory card. Camera images are stored in their native Bayer-16 format, and are converted to TIFF images by a batch

process after the SES has been recovered. This reduces data storage requirements, as the Bayer-16 images are about one-third the size of the TIFF images (10 MB vs. 30 MB), and it conserves the battery energy that would be required to convert the images in situ. The vast majority of data storage is taken up by camera images, with the remainder used for fluorometer readings and engineering data such as battery voltage. The software also maintains extensive log files to record every action taken by the SES in order to verify correct operation and to help determine the cause of any malfunction.

Assessment

Testing

The SES was first tested in the 1.5 million liter, 10 m deep saltwater tank at the Monterey Bay Aquarium Research Institute to verify basic functionality. This test also enabled adjustment of the LED light intensities for optimal camera exposure in water.

After tank testing, the SES was deployed on the Monterey Accelerated Research System (MARS) cabled observatory in Monterey Bay, 37 km from shore at a depth of 900 m (Henthorn et al. 2010). Cable interface electronics were installed in the SES battery housing to allow the instrument to receive power and data connections from the MARS network, permitting shore-based researchers to control the SES and receive images in real time. This capability proved to be invaluable as repeated cycling revealed an infrequent but serious flaw in the sample plate cleaning mechanism, causing the carousel to jam in a way that could not be corrected without recovery of the instrument. The SES was recovered and redeployed two more times on MARS before modifications to the sample

mechanism were deemed reliable enough for autonomous deployment at greater depths offshore.

Station M deployments

In June 2012, the SES was deployed at Station M (34° 50' N, 123° 00' W), a long-term study site located 220 km offshore of the central California coast (Smith et al. 2013). A mooring held the SES at a depth of 3910 m, 50 m above the seafloor at 3960 m depth. Local resuspension of bottom sediments does not appear to be a significant source of carbon at this depth (Bianchi et al. 1998; Druffel et al. 1998; Sherrell et al. 1998; Smith et al. 2001). In addition to vertical

transport, easterly lateral transport from the distant continental margin can be important based on the higher percentage of refractory organic material (Bianchi et al. 1998). This site has been the focus of a long time-series monitoring program since 1989. Other instruments at the study site include a wide-area seafloor time-lapse camera, a benthic rover vehicle, and traditional sediment traps.

For the first Station M deployment the SES was programmed to process a sample every 12 h. When the instrument was recovered in November 2012, it had processed a total of 304 samples, the expected number for the 5-month deployment. Initial inspection of the images revealed times when the sample plate was completely covered with sediment, resulting in some images being almost completely dark. Because fully dark images obscured individual particle interpretation, the sample interval was reduced to 3 h for the second deployment in November 2012, aiming to collect less material per image. When the instrument was serviced after another 7 months in June 2013, it had processed an additional 1200 samples, stopping as programmed before the battery was depleted. The third SES deployment was the longest, lasting 10 months from June 2013 until April 2014.

Table 1. Samples processed on first three deployments of sedimentation event sensor.

Deploy number	Duration	Sample interval	Collection time	Samples processed
1	5 months	12 h	12 h	304
2	7 months	3 h	3 h	1200
3	10 months	4 h	2 h	1420

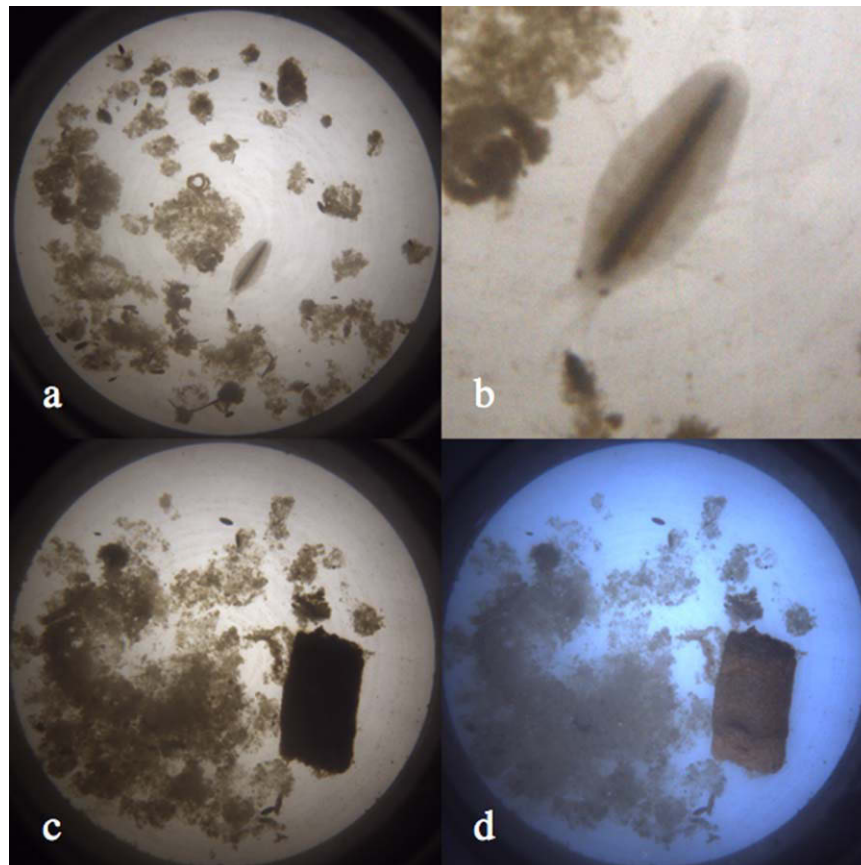


Fig. 7. Sample images from SES deployment at Station M: (a) Typical sample with a variety of organic material on the 25 mm diameter sample plate; (b) Detail of sample in panel (a) showing a small crustacean about 3.9 mm long with legs and gut visible; (c) Back-lit image with a large rectangular salp fecal pellet; (d) Front-lit image of sample shown in panel c, showing more detail of the same salp fecal pellet.

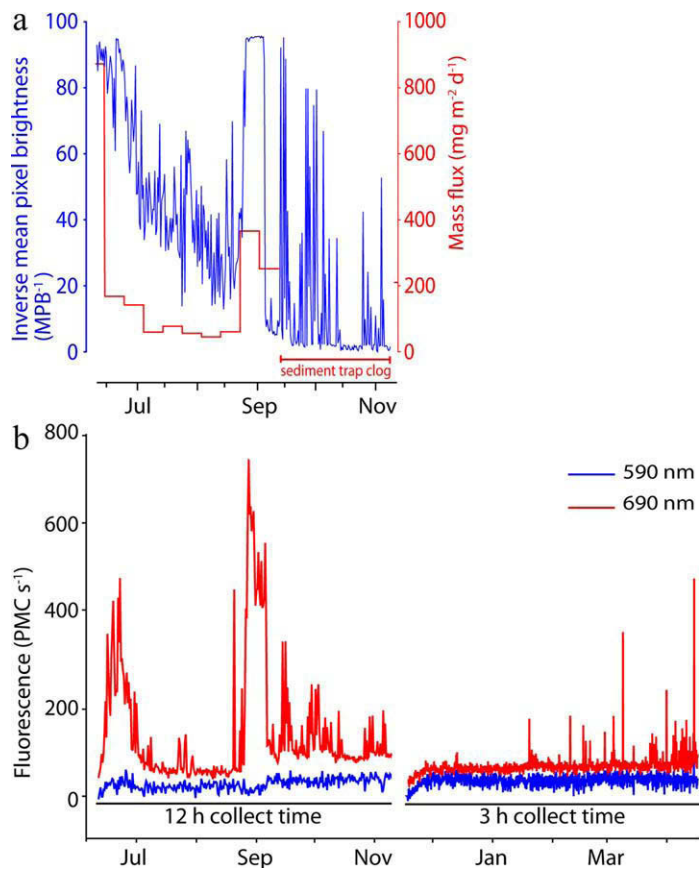


Fig. 8. SES data collected at Station M in 2012. **(a)** Relative sediment quantity collected by the SES determined by measuring the inverse mean brightness value of the sample plate images (blue line and axis) based on fluorescence readings. Sedimentation rates determined by the SES were comparable to mass flux measured by concurrently deployed sediment traps at the same station and depth (red axis and line). **(b)** Fluorometer readings during two consecutive deployments with different collect times. The vertical axis values are photomultiplier counts per second. Sustained periods of material fluorescent in the 690 nm band (Chl *a*) were seen during the first deployment, but not during the second deployment.

The SES recorded a total of 1420 samples processed at 4 h intervals, stopping only when the flash memory card filled. For the first two deployments, the collection time was equal to the sample interval (12 h and 3 h respectively). However, the collection time was reduced to only half the sample interval for the third deployment (2 h collect, 2 h standby) with the carousel in a flow-through position that collects no sediment for the remainder of each sample interval. These results are summarized in Table 1.

Results

Images

The macro photographs revealed detail about the size distribution and composition of collected sediments. Figure 7 shows typical images. Most of the material on the sample

plate consisted of aggregations of phytodetritus along with fecal pellets of various types and sizes. Sometimes a whole animal was collected, such as the small crustacean seen in panels 7a and 7b. The backlight provided the best illumination for interpreting most of the images. For instance, the gut of the crustacean is clearly visible in panel 7b. However large, opaque objects such as the salp fecal pellet in panel 7c were best viewed with front lighting, as seen in panel 7d. Note the blue tint of the background light in the front-lit image, but not the back-lit image. Both the front and back lights use the same type of white LED, but only the back-light passes through the sample plate material, absorbing the shorter wavelengths.

Although a detailed analysis of each SES image can be made, it is also possible to make simpler measurements in order to get a broad perspective of sedimentation rates during a deployment. Figure 8a shows the inverse mean pixel brightness (MPB⁻¹) of each image recorded between June and November of 2012. This value was determined using image analysis functions of Mathematica 10.4 to arrive at each image's mean pixel brightness (MPB). We then took the inverse of MPB, and scaled MPB⁻¹ such that an empty sample plate, representing the brightest image possible, has a value of 0 and a completely black image has a value of 100%. The sample plate most completely covered with material at Sta. M had a MPB⁻¹ value of about 95%. Although this sample plate was completely covered with material, a small amount of light still leaked through the sample. This value conceptually gives a relative measure of sample opacity and light attenuation, which depend on particulate composition, surface area of the sample plate covered by material, and layer thickness. From the time series of MPB⁻¹ (Fig. 8a) we could see that sedimentation rates were quite high at the beginning of the deployment, then diminished through June, July, and the first half of August 2012. In the last week of August, a pulse of material was detected with a sudden onset and conclusion, lasting about 10 d. This pulse of material was followed by highly variable sedimentation rates from mid-September to mid-October. Almost no material was collected during the third week of October, and then episodic pulses of material were seen until the end of the deployment in the first week of November.

Sedimentation rates as determined by the SES were compared to those from a traditional sediment trap operating at Station M during the same period. Both sampling methods were moored 50 m above bottom, but kilometers apart. Sample bottles from the traditional trap were filled with a formalin mixture and collected at 10-d intervals (Smith et al. 2013). Samples were returned to the lab, freeze-dried, and then weighed to determine the total dry mass of collected material. Mass flux ($\text{mg m}^{-2} \text{d}^{-1}$) was calculated using this measure, divided by the funnel opening size (0.5 m^2) and the collection time. The red line in Fig. 8a represents the average quantity of sediment collected daily during each 10-

d period. No mass flux data are available for the months of September or October 2012 due to a clog in the traditional sediment traps. Clogging and subsequent clearing are recurring problems with traditional sample collection that the SES is intended to, and did, ameliorate. For the times when both instruments collected material contemporaneously, the same general trends in sedimentation rates were seen. There were differences, but this is to be expected because they differed in exact location and collect time. Additionally, because collected material can be comprised of overlaying layers of particles with different transparency, we cannot assume that our proxy for light attenuation yields a linear proxy for material mass (Estapa et al. 2013; Bishop et al. 2016).

Fluorometry

We analyzed fluorometer data collected using a 1 s integration time. Figure 8a shows the fluorometer record from the first two deployments, spanning a time period of 11 months. The collection time of material through the funnel was 12 h for the first deployment and 3 h for the second deployment, so γ -axis values cannot be directly compared between the two deployments for scientific interpretation. General features of activity during the period, however, can be observed.

The gap in November between the two deployments is the time that the SES was on the ship being serviced. The first week of each deployment showed a slow change in fluorescence, starting at zero and increasing over a period of about a week to more typical levels. Examination of the first week of images from each deployment revealed condensation on the optical viewports of the instrument housings, despite the use of desiccant and dry-nitrogen purging of the housings. Deployment procedures have since been modified to increase both the quantity of desiccant and the time of the dry-nitrogen purging in order to rectify this problem.

Two pulses of material possibly bearing Chl *a* can be seen on the 690 nm record in June, and again from late August to early September of 2012. These times corresponded to the periods of the highest sedimentation rates seen in Fig. 8a, as well as record-high depositions of salp fecal-pellets recorded by the sediment traps, and salp tunics and phytodetritus on the sea floor at Station M as detected by a benthic rover (Smith et al. 2014). Note however that during July and August, when sedimentation rates were still quite high, fluorescence was low. This result implies that material collected during those times had a fundamentally different composition than that collected during the other pulse events. Salp tunics and fecal pellets were visible in the SES images more commonly during this first pulse than other periods. The second deployment showed no sustained pulses of fluorescent material, however extremely brief pulses, comprising a single sample each, were seen. No significant activity was evident on the 590 nm record for either deployment, nor

was any luminescence or phosphorescence seen when the fluorometer excitation source was switched off.

Discussion

The SES has proven to be a reliable instrument, processing 2924 samples on its first three deployments with no malfunctions. This reliability was achieved through rigorous testing on the MARS cabled observatory at 900 m depth before long-term deployment in deeper water. Design and construction of the SES was greatly facilitated by basing it upon a proven commercial sediment trap. Custom power control circuitry allows the system electronics to be built from inexpensive commercial microcontroller boards and peripherals, and greatly shortened the hardware development time. The use of the open-source Linux operating system and Ruby programming language also help to lower system costs.

Initial examination of the data from these deployments has revealed that both the deposition rate and composition of settling particulate matter at Station M is highly variable on time scales as short as a few hours. While the SES does provide high-resolution images of the collected samples, it does not retain those samples and thus cannot provide direct measures of mass flux or further analysis of carbon content. Flux values generated from the SES will need to be estimated from models based on concurrent sediment trap and SES sampling periods. However, the SES can measure the fluorescence of the samples in situ, where this information is lost in the stored samples of a traditional sediment trap (Vaulot et al. 1989). Phytodetritus is a high-quality food source for deep-sea communities (Fitzgeorge-Balfour et al. 2010), so the ability to estimate the chlorophyll content of settling material has strong scientific value. Given these functional differences, the SES is best used to complement rather than replace traditional sediment traps.

We are aware of one other sediment trap that uses a camera to record and analyze sediment in situ. The Carbon Flux Explorer (Bishop 2009) was first deployed in 2007 to measure aspects of sinking particulate matter while avoiding the necessity of sample retrieval. It increases both deployment duration and sampling frequency beyond that of traditional sediment traps, but differs from the SES in its deployment modes. The Carbon Flux Explorer integrates an Optical Sedimentation Recorder with a Sounding Oceanographic Lagrangian Observer float to produce images used to estimate both particulate organic carbon and particulate inorganic carbon fluxes in the upper 1000 m of the water column (Bishop et al. 2016). Its optical sedimentation recorder uses a camera with multiple light sources to image particles collected on a horizontal optical window. After the images are taken in situ, the instrument surfaces and Global Positioning System position, engineering data, and conductivity, image thumbnails, and temperature and depth profile

Table 2. Comparison of sedimentation event sensor and carbon-flux explorer (Bishop 2009; Bishop et al. 2016).

	Sedimentation event sensor	Carbon flux explorer
Deployment method	Moored	Free-drifting
Sample illumination	Front, back	Back (non- and cross-polarized), side
Fluorometry	Yes	No
Samples per deployment	6200	~2000
Real-time data recovery	No	Yes
Full-resolution images recovered	Yes	No, unless drifter recovered

data are sent to shore via satellite (Bishop 2009; Bishop et al. 2016). Full resolution images obtained upon recovery of the instrument are used to estimate particulate organic carbon and particulate inorganic carbon fluxes (Bishop et al. 2016). This vertically profiling float is autonomous and Lagrangian, capable of analyzing samples every half hour for 1–2 months. While suitable for drift studies with large geographic coverage, the Carbon Flux Explorer is less appropriate for prolonged studies at a single station, and at abyssal sites. Table 2 outlines the respective capabilities of the Carbon Flux Explorer and the SES.

Future work with the SES includes adding battery capacity and memory storage to increase the deployment time beyond a year, further reducing the use of expensive ship time spent servicing the instrument. A shorter and simpler version of the SES frame, eliminating the drop-weight mechanism, would allow the instrument to be deployed anywhere along a mooring string, from midwater to shallow depths. The SES software permits the sampling interval and collection time to be varied easily, although the optimum settings will depend upon location and season. Enhanced instrument software could set the collection time dynamically during the deployment based upon a density analysis of the previous sample image, although material collected with non-uniform collection times would be more difficult to analyze quantitatively. The current platform invites the development of additional sensors, such as an imaging fluorometer to reveal more detail about the composition of collected samples.

References

Bianchi, T. S., J. E. Bauer, E. R. Druffel, and C. D. Lambert. 1998. Pyrophaeophorbide-a as a tracer of suspended particulate organic matter from the NE Pacific continental margin. *Deep-Sea Res. Pt. II* **45**: 715–731. doi:[10.1016/S0967-0645\(97\)00099-4](https://doi.org/10.1016/S0967-0645(97)00099-4)

Bishop, J. K. B. 2009. Autonomous observations of the ocean biological carbon pump. *Oceanography* **22**: 182–193. doi:[10.5670/oceanog.2009.48](https://doi.org/10.5670/oceanog.2009.48)

Bishop, J. K. B., M. B. Fong, and T. J. Wood. 2016. Robotic observations of high wintertime carbon export in California coastal waters. *Biogeosciences* **2016**: 1–32. doi:[10.5194/bg-2016-62](https://doi.org/10.5194/bg-2016-62)

Buesseler, K. O., and others. 2007. An assessment of the use of sediment traps for estimating upper ocean particle fluxes. *J. Mar. Res.* **65**: 345. doi:[10.1357/002224007781567621](https://doi.org/10.1357/002224007781567621)

Druffel, E. R. M., S. Griffin, J. E. Bauer, D. M. Wolgast, and X.-C. Wang. 1998. Distribution of particulate organic carbon and radiocarbon in the water column from the upper slope to the abyssal NE Pacific Ocean. *Deep-Sea Res. Pt. II* **45**: 667–687. doi:[10.1016/S0967-0645\(98\)00002-2](https://doi.org/10.1016/S0967-0645(98)00002-2)

Earp, A., and others. 2011. Review of fluorescent standards for calibration of in situ fluorometers: Recommendations applied in coastal and ocean observing programs. *Opt. Express* **19**: 26768–26782. doi:[10.1364/OE.19.026768](https://doi.org/10.1364/OE.19.026768)

Estapa, M. L., K. Buesseler, E. Boss, and G. Gerbi. 2013. Autonomous, high-resolution observations of particle flux in the oligotrophic ocean. *Biogeosciences* **10**: 5517–5531. doi:[10.5194/bg-10-5517-2013](https://doi.org/10.5194/bg-10-5517-2013)

Fitzgeorge-Balfour, T., D. S. M. Billett, G. A. Wolff, A. Thompson, and P. A. Tyler. 2010. Phytopigments as biomarkers of selectivity in abyssal holothurians; interspecific differences in response to a changing food supply. *Deep-Sea Res. II* **57**: 1418–1428. doi:[10.1016/j.dsr2.2010.01.013](https://doi.org/10.1016/j.dsr2.2010.01.013)

Henthorn, R. G., B. W. Hobson, P. R. McGill, A. D. Sherman, and K. L. Smith. 2010. Mars benthic rover: In-situ rapid proto-testing on the monterey accelerated research system. *OCEANS 2010 MTS/IEEE SEATTLE*, Seattle, WA, 2010: 1–7. doi:[10.1109/OCEANS.2010.5664381](https://doi.org/10.1109/OCEANS.2010.5664381)

Honjo, S. 1980. Material fluxes and modes of sedimentation in the mesopelagic and bathypelagic zones. *J. Mar. Res.* **38**: 53–97.

Honjo, S., and K. W. Doherty. 1988. Large aperture time-series sediment traps; design objectives, construction and application. *Deep-Sea Res. A* **35**: 133–149. doi:[10.1016/0198-0149\(88\)90062-3](https://doi.org/10.1016/0198-0149(88)90062-3)

Knauer, G. A., J. H. Martin, and K. W. Bruland. 1979. Fluxes of particulate carbon, nitrogen, and phosphorus in the upper water column of the northeast Pacific. *Deep-Sea Res. A* **26**: 97–108. doi:[10.1016/0198-0149\(79\)90089-X](https://doi.org/10.1016/0198-0149(79)90089-X)

Sherrell, R. M., M. P. Field, and Y. Gao. 1998. Temporal variability of suspended mass and composition in the Northeast Pacific water column: Relationships to sinking flux and lateral advection. *Deep-Sea Res. Pt. II* **45**: 733–761. doi:[10.1016/S0967-0645\(97\)00100-8](https://doi.org/10.1016/S0967-0645(97)00100-8)

Smith, K. L., R. S. Kaufmann, Jr., R. J. Baldwin, and A. F. Carlucci. 2001. Pelagic–benthic coupling in the abyssal eastern North Pacific: An 8-year time-series study of food supply and demand. *Limnol. Oceanogr.* **46**: 543–556. doi:[10.4319/lo.2001.46.3.0543](https://doi.org/10.4319/lo.2001.46.3.0543)

Smith, K. L., H. A. Ruhl, Jr., M. Kahru, C. L. Huffard, and A. D. Sherman. 2013. Deep ocean communities impacted by

- changing climate over 24 y in the abyssal northeast Pacific Ocean. *Proc. Natl. Acad. Sci. U.S.A.* **110**: 19838–19841. doi:[10.1073/pnas.1315447110](https://doi.org/10.1073/pnas.1315447110)
- Smith, K. L., others. 2014. Large salp bloom export from the upper ocean and benthic community response in the abyssal northeast Pacific: Day to week resolution. *Limnol. Oceanogr.* **59**: 745–757. doi:[10.4319/lo.2014.59.3.0745](https://doi.org/10.4319/lo.2014.59.3.0745)
- Vaulot, D., C. Courties, and F. Partensky. 1989. A simple method to preserve oceanic phytoplankton for flow cytometric analyses. *Cytometry* **10**: 629–635. doi:[10.1002/cyto.990100519](https://doi.org/10.1002/cyto.990100519)
- Yentsch, C. S., and D. A. Phinney. 1985. Spectral fluorescence: An ataxonomic tool for studying the structure of phytoplankton populations. *J. Plankton Res.* **7**: 617–632. doi:[10.1093/plankt/7.5.617](https://doi.org/10.1093/plankt/7.5.617)

Acknowledgments

The authors thank Rob Glatts and Fred Uhlman for their work on an earlier version of the SES at the Scripps Institution of Oceanography. Funding was provided by NSF Grants OCE0242472 and OCE0638505 and by the David and Lucile Packard Foundation.

Submitted 14 April 2016

Revised 28 June 2016

Accepted 12 July 2016

Associate editor: Clare Reimers